Distributed Online Voltage Control in Distribution Network: A Two-stage Real-time Implementation

Zhengfa Zhang, *Member*, *IEEE*, Filipe Faria da Silva, *Senior Member*, *IEEE*, Yifei Guo, *Member*, *IEEE*, Yufei Xi, *Member*, *IEEE*, Claus Leth Bak, *Senior Member*, *IEEE*, Jose Rueda Torres, *Senior Member*, *IEEE*, Jin Dong, *Member*, *IEEE*, Zhe Chen, *Fellow*, *IEEE*, and Yilu Liu, *Fellow*, *IEEE*

***Abstract*—The increasing integration of renewable-based distributed generation (DG) brings growing challenges to distribution network (DN) voltage control. To address this issue, a two-stage distributed online voltage control framework (TDO-VC) is proposed in this paper. In the proposed method, legacy voltage control devices are controlled in the upper stage on an hourly timescale, while DGs operate autonomously online in the lower stage to remove instantaneous voltage violations. The idea of receding horizon control is applied in the upper stage to comprehensively consider the current and future renewable generation, and the generalized fast dual ascent (Gf-DA) is employed in the lower stage to effectively manage DGs through near real-time optimization. The effectiveness of the proposed TDO-VC is demonstrated by rigorous theoretical analysis and case studies on IEEE-123 bus system.**

***Index Terms*—Distributed generation, distributed online control, distribution network, generalized fast dual ascent, receding horizon control, voltage control.**

NOMENCLATURE

A. Abbreviations

ADMM	Alternating direction method of multipliers.
CB	Capacitor bank.
DG	Distributed generation.
DA	Dual Ascent.
DN	Distribution network.
Gf-DA	Generalized fast dual ascent.
LSC	Lower stage controller.
OLTC	On-load tap changer.
TDO-VC	Two-stage distributed online voltage control.
USC	Upper stage controller.
VVC	Voltage/var control.

B. Variables

p_i, q_i	Real/reactive power injection at node i.
$\boldsymbol{p}, \boldsymbol{q}$	Vector of real/reactive power injection.
P_{ij}, Q_{ij}	Real/reactive power flow over branch (i, j).
$\boldsymbol{p}_{\rm l}$, $\boldsymbol{q}_{\rm l}$	Vector of real/reactive power load consumption.
$\boldsymbol{p}_{\rm inv}$, $\boldsymbol{q}_{\rm inv}$	Vector of DG real/reactive power injection.
$\overline{\boldsymbol{q}}_{\rm inv}, \underline{\boldsymbol{q}}_{\rm inv}$	Vector of max/min DG reactive power limits.
$\boldsymbol{n}_{\rm tap}, \boldsymbol{n}_{\rm c}$	Vector of OLTC/CB tap position.
$\boldsymbol{q}_{\rm c}$	Vector of reactive power injection of CB.
k	Iteration step.
v_i	Squared voltage magnitude at bus i.
$\boldsymbol{v}$	Vector of squared voltage magnitude.
$\overline{\boldsymbol{v}}, \underline{\boldsymbol{v}}$	Vector of max/min voltage limit.
$\overline{\boldsymbol{n}}_{\rm tap}, \underline{\boldsymbol{n}}_{\rm tap}$	Vector of max/min OLTC tap position.
$\overline{\boldsymbol{n}}_{\rm c}$	Vector of max CB tap position.
$\Delta\overline{\boldsymbol{n}}_{\rm c}, \Delta\underline{\boldsymbol{n}}_{\rm c}$	Vector of max/min CB tap position change per step.
$\Delta\overline{\boldsymbol{n}}_{\rm tap}$, $\Delta\underline{\boldsymbol{n}}_{\rm tap}$	Vector of max/min OLTC tap position change per step.
$\overline{\boldsymbol{\mu}}, \underline{\boldsymbol{\mu}}$	Dual vectors associated with voltage limits.
$\overline{\boldsymbol{\lambda}}, \underline{\boldsymbol{\lambda}}$	Dual vectors associated with reactive power limits.
$\overline{\boldsymbol{\omega}}, \underline{\boldsymbol{\omega}}$	Auxiliary vectors associated with $\overline{\boldsymbol{\mu}}, \underline{\boldsymbol{\mu}}$.
$\overline{\boldsymbol{\eta}}, \underline{\boldsymbol{\eta}}$	Auxiliary vectors associated with $\overline{\boldsymbol{\lambda}}, \underline{\boldsymbol{\lambda}}$.
$S_{\rm inv}$	Capacity of DG inverter.

C. Parameters

$\bar{\boldsymbol{A}}$	Graph incidence matrix of network.
$\boldsymbol{A}$	Reduced graph incidence matrix.
$\boldsymbol{D}_r$	Diagonal branch resistance matrix.
$\boldsymbol{D}_x$	Diagonal branch reactance matrix.
$L, \boldsymbol{L}$	Lipschitz constant and its generalization.
r_{ij}, x_{ij}	Resistance/reactance of branch (i, j).
$n_{\rm tap}$	Voltage change per OLTC step.
$v_{\rm nom}$	Squared nominal voltage magnitude.
$\omega_{\rm mec}$, ω_v	Weighting factor of mechanical VVC devices/ voltage regulation.
$c_{\rm tap}$, $c_{\rm c}$	Cost of OLTC/CB step change.
$n_{\rm tap}$	Voltage change per OLTC step.
$\Delta q_{\rm c}$	Reactive power injection per CB step.

Manuscript received October 19, 2024; revised January 26, 2025; accepted February 27, 2025. Date of online publication May 16, 2025; date of current version July 18, 2025. This work was supported by UT-Battelle, LLC under Contract DE-AC05-00OR22725 with the U.S. Department of Energy (DOE), and supported in part by the DOE Solar Energy Technologies Office (SETO).

Z. F. Zhang and Y. L. Liu are with Department of Electrical Engineering and Computer Science, University of Tennessee Knoxville, Knoxville, TN 37996, USA.

F. F. da Silva, C. L. Bak and Z. Chen are with the Department of Energy Technology, Aalborg University, 9220 Aalborg, Denmark.

Y. F. Xi (corresponding author, email: xyfneepu@outlook.com) is with State Key Laboratory of Power System Operation and Control, Tsinghua University, Beijing 100084, China.

Y. F. Guo is with School of Engineering, University of Aberdeen, UK.

J. R. Torres is with Department of Electrical Sustainable Energy, Technical University Delft, Netherlands.

J. Dong is with the Oak Ridge National Laboratory, Oak Ridge, TN 37831, USA.

DOI: 10.17775/CSEEJPES.2024.08000

$\boldsymbol{I}_N$	$N \times N$ identity matrix.
$\mathbf{1}_N$	$N \times 1$ vector with all entries being 1.
$\mathbf{0}_N$	$N \times 1$ vector with all entries being 0.

D. Sets

$\mathcal{L}$	Set of branches.
$\mathcal{N}$	Set of buses.
$\mathcal{C}_j$	Set of children buses of bus j.
$\mathcal{N}_i$	Set of neighbors of node i in cyber layer.

I. Introduction

NOWADAYS, renewable energy is playing a more and more important role in the energy patterns [1], [2]. A large percentage of renewable energy is being integrated into DNs in the form of DG. The renewable generation is inherently time-varying sources with stochastic and intermittent features, which leads to rapid voltage fluctuation or even voltage violation in DNs [3].

The main task of voltage/var control (VVC) is to maintain the DN bus voltages within the allowed limit. Traditionally, VVC is accomplished by adjusting the utility-owned legacy voltage regulation devices, such as transformer with on-load tap changer (OLTC) and capacitor banks (CBs). However, these mechanical devices may be less effective to tackle the VVC control challenges in scenarios with high renewable penetration [4]. Therefore, the fast-acting power electronics interfaced DGs are required to provide flexible voltage support, as advocated by the amended IEEE 1547 standard [5], [6].

Up to now, a number of technical solutions have been proposed to address the above voltage control issue, as summarized in Table I. These solutions can be roughly classified into following three groups: local, centralized and distributed. The control actions in local control are updated by a local control rule, e.g. droop control [7], proportional and integral control [8], adaptive control [9] etc. Local methods can be implemented online and adapted to fast dynamics in real-time; however, they often suffer from degraded performance because they rely only on local measurements [10]. By contrast, in centralized methods, the control center gathers the network-wide information and performs optimal power flow calculation in a fixed time period (typically, 15 min), then sends the control commands based on the optimization results. For example, the voltage regulation devices were controlled in two separate timescales in [11] and [12], considering different characteristics of the devices. Multi-stage stochastic programming and robust optimization were used in [13] and [14] respectively, to address the uncertainties introduced by integration of renewable generation. The optimality can be achieved in centralized control by resorting to centralized controller and complex communication. However, the computational burden could be heavy and system reliability is threatened, particularly for large scale DNs. In addition, the centralized design is not suitable for tackling fast voltage disturbances.

Distributed control methods have been proposed to reduce the communication complexity and enhance the voltage control reliability by replacing centralized controller with several sub-controllers [15]. A distributed leader-followers control method was presented in [16] to achieve conservation voltage reduction by scheduling DG inverters. Alternating direction method of multipliers (ADMM) was used to develop distributed framework in [17], the outputs of PV inverters were adjusted to regulate the bus voltages by information exchange between adjacent DN areas. An improved ADMM was used in [18] by taking into the legacy voltage regulating devices into consideration that the traditional ADMM was not able to handle. Nevertheless, these distributed works are still based on off-line computing, thus not suitable for online control.

Distributed online voltage control has attracted growing attention in recent years as it can adapt to fast-varying system dynamic condition with relatively low communication requirements [19], [20]. In [19], the primal-dual gradient algorithm was used to realize real-time voltage control, where each agent makes its decision by local voltage measurement and communication with physical connected neighbours. In [20], dual ascent (DA) algorithm was employed to eliminate voltage violation and minimize power losses in unbalanced DNs. However, the slow convergence of conventional gradient methods is a hurdle for fast voltage control. In addition, the coordination of the online algorithm with legacy voltage regulating devices was not well addressed in these works.

To fill the research gap of current research, we propose a two-stage distributed online voltage control framework in this paper. In the proposed framework, the mechanical devices are dispatched in the upper stage with longer timescale to cope with the voltage variation caused by intraday change of load/generation profile. In the lower stage, the DGs operate autonomously to remove instantaneous voltage violation and minimize power losses in real-time. The lower stage control of DGs is realized by applying the Gf-DA algorithm. In the

TABLE I
COMPARISON OF DIFFERENT VOLTAGE CONTROL METHODS

Aspects	Centralized method	Local method	Distributed Method	Proposed Method
Communication requirements	Requires complex communication between centralized controller and nodes	No communication required	Moderate communication among agents	Low communication requirements between neighouring buses
Response time	Slow	Fast	Moderate	Fast
Robustness	Susceptible to communication failure	High	Moderate due to decentralized implementation	Robust to communication failure
Optimal	Global optimal	Suboptimal due to local nature	Near-global optimal	Near-global optimal
Cost	High, due to centralized hardware and software infrastructure	Low, due to simple implementation	Moderate, requires distributed controllers and limited communication	Moderate, due to low communication and computation requirements

author's previous work [21], Gf-DA is applied in a wind farm scenario, aiming at minimizing the voltage deviations and maintaining adequate VAR reserves. In this work, we explore the application of Gf-DA to distribution network voltage control, aiming at minimizing network power losses and regulating the bus voltages in the allowed range. In addition, we develop a two-stage distributed online voltage control framework in which the upper stage control of legacy voltage control equipment and the lower stage control of distributed generations are coordinated.

Compared with the existing works in this area, the contributions of this paper are summarized as follows:

1) The schedule of legacy voltage regulating devices and the online control of DGs is coordinated. The tap positions of legacy voltage control devices are dispatched in the upper stage while in the lower stage, DGs cooperate autonomously in real-time to realize effective voltage control and minimize power losses.

2) The idea of receding horizon control is applied in the upper stage by taking into consideration of both current and forecasted value of renewable generation. In the lower stage, the Gf-DA with fast convergence is employed to facilitate the online implementation. Both simulation verification and rigorous theoretical analysis on the convergence rate are provided.

3) The proposed TDO-VC has reduced communication complexity compared with centralized control and is robust to communication failure and model errors.

The remainder of this paper is organized as follows: Section II introduces the modeling of DNs. The voltage control problem is formulated in Section III. The distributed online voltage control design is presented in Section IV. Case studies are presented in Section V, followed by conclusion remarks in Section VI.

II. Preliminaries

As shown in Fig. 1, the topology of typical radial DN is represented by $\mathcal{G} = (\mathcal{N}, \mathcal{L})$, where $\mathcal{N} := \{0, 1, \cdots, N\}$ denotes set of buses while $\mathcal{L} := \{1, \cdots, N\}$ denotes set of branches. For each bus $i \in \mathcal{N}$, let $s_i = p_i + \boldsymbol{i} q_i$ denote its complex power injection. For each branch $(i, j) \in \mathcal{L}$, let $z_{ij} = r_{ij} + \boldsymbol{i} x_{ij}$ denote its impedance and $S_{ij} = P_{ij} + \boldsymbol{i} Q_{ij}$ be the complex power flowing from bus i to j. Then, the power flow can be represented by the linear Distflow equation:

$$P_{ij} = \sum_{k \in \mathcal{C}_j} P_{jk} - p_j \tag{1a}$$

$$Q_{ij} = \sum_{k \in \mathcal{C}_j} Q_{jk} - q_j \tag{1b}$$

$$v_i - v_j = 2(r_{ij} P_{ij} + x_{ij} Q_{ij}) \tag{1c}$$

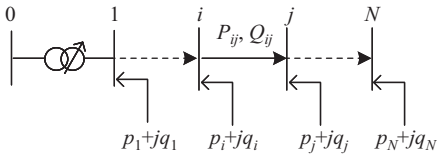

Fig. 1. Topology of DN.

For branches with OLTC on the secondary side, (1c) can be modified as:

$$t_{ij}^2 v_i - v_j = 2(r_{ij} P_{ij} + x_{ij} Q_{ij}) \tag{1d}$$

where t_{ij} represents the OLTC tap ratio. Substituting $t_{ij} = 1 + n_{\text{tap},ij} \Delta\text{tap}_{ij}$ and further linearizing (1d) into (1e) [22],

$$v_i - v_j = 2(r_{ij} P_{ij} + x_{ij} Q_{ij}) - 2 n_{\text{tap},ij} \Delta\text{tap}_{ij} v_{\text{nom}} \tag{1e}$$

The linear Distflow model can be organized into compact form for conciseness. Firstly, define the incidence matrix of $\mathcal{G}$ as $\bar{\boldsymbol{A}} = [\boldsymbol{a}_0 \ \boldsymbol{A}^{\mathrm{T}}]^{\mathrm{T}} \in \{0, \pm 1\}^{(N+1)\times N}$, which is defined as: $\bar{\boldsymbol{A}}_{il} = 1$ if branch l starts at bus i and $\bar{\boldsymbol{A}}_{il} = -1$ if branch l ends at bus i, otherwise $\bar{\boldsymbol{A}}_{il} = 0$. $\boldsymbol{a}_0^{\mathrm{T}}$ is the first row of $\bar{\boldsymbol{A}}$ while $\boldsymbol{A}$ is the remaining submatrix. Then the compact form representation of (1e) can be given as:

$$[\boldsymbol{a}_0 \ \ \boldsymbol{A}^{\mathrm{T}}] \begin{bmatrix} v_0 \\ \boldsymbol{v} \end{bmatrix} = 2(\boldsymbol{D}_r \boldsymbol{P} + \boldsymbol{D}_x \boldsymbol{Q}) - 2 v_{\text{nom}} \Delta\text{tap} \boldsymbol{n}_{\text{tap}} \tag{2}$$

where $\boldsymbol{D}_r := \text{diag}(\boldsymbol{r}) \in \mathbb{R}^{N\times N}$ with ℓ_th diagonal equals to r_{ij} of the ℓ_th branch $\in \mathcal{L}$, the same with $\boldsymbol{D}_x := \text{diag}(\boldsymbol{x}) \in \mathbb{R}^{N\times N}$. Equation (2) can be equivalent given as:

$$\boldsymbol{v} = \boldsymbol{R}\boldsymbol{p} + \boldsymbol{X}\boldsymbol{q} + v_0 \boldsymbol{1}_N - 2 v_{\text{nom}} \Delta\text{tap} \boldsymbol{A}^{-\mathrm{T}} \boldsymbol{n}_{\text{tap}} \tag{3}$$

where $\boldsymbol{1}_N$ is N-dimension all-ones vector and

$$\boldsymbol{R} = 2\boldsymbol{A}^{-\mathrm{T}} \boldsymbol{D}_r \boldsymbol{A}^{-1} \tag{4a}$$

$$\boldsymbol{X} = 2\boldsymbol{A}^{-\mathrm{T}} \boldsymbol{D}_x \boldsymbol{A}^{-1} \tag{4b}$$

III. Formulation of Voltage Control Problem

In this section, we introduce the details of the proposed TDO-VC framework. Considering that the response speed of legacy VVC devices is much slower than that of DG inverters, a two-stage voltage controller is applied in the proposed TDO-VC to dispatch different VVC devices. The coordination of upper stage controller and lower-stage controller is illustrated in Fig. 2. In the proposed TDO-VC, the tap positions of OLTC and CBs are dispatched with longer time scale in the upper stage, while the reactive power output of DG inverters is adjusted in the lower stage online in real-time by information exchange among neighboring buses.

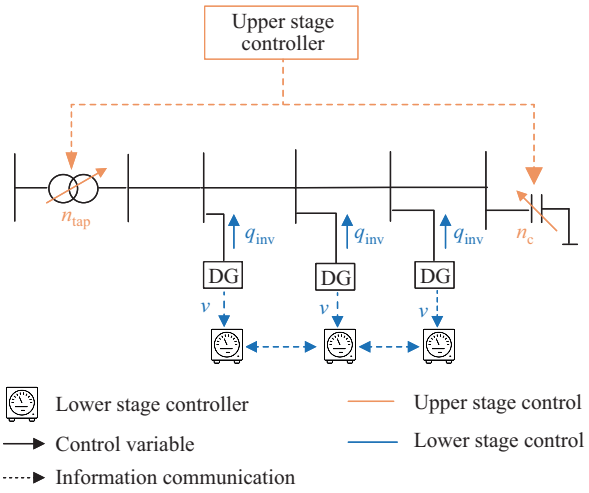

Fig. 2. Diagram of the two-stage voltage controller.

A. Upper Stage Controller

The upper stage controller (USC) is dispatched hourly ahead by resorting to the idea of receding horizon control. The advantage of receding horizon control is that it can comprehensively consider both the current and forecast values to improve the algorithm performance. The main objective of USC is to track the intraday change of generation and load profile by dispatching the tap positions of OLTC and CBs in an hour ahead manner. As the high penetration of renewable generation often leads to more frequent operation of mechanical VVC devices, which is detrimental to their lifespan. So the objectives of USC is to reduce the operation of tap positions of OLTC and CBs, as well as regulating the bus voltages close to nominal value. The mathematical formulation of USC is given as:

$$\min_{\boldsymbol{n}_{\rm tap},\boldsymbol{n}_{\rm c},\boldsymbol{q}_{\rm inv}} \sum_{i=t+1}^{i=t+N_p} \begin{array}{l}[\omega_{\rm mec}(c_{\rm tap}\|\boldsymbol{n}_{\rm tap}(i)-\boldsymbol{n}_{\rm tap}(i-1)\|_2 \\ \quad +c_{\rm c}\|\boldsymbol{n}_{\rm c}(i)-\boldsymbol{n}_{\rm c}(i-1)\|_2) \\ \quad +\omega_v(\boldsymbol{v}(i)-v_{\rm nom})]\end{array} \tag{5a}$$

subject to

$$\begin{aligned}\boldsymbol{v}(i) = \boldsymbol{R}\boldsymbol{p}(i) + \boldsymbol{X}\boldsymbol{q}(i) + v_0\mathbf{1}_N \\ - 2v_{\rm nom}\Delta{\rm tap}\boldsymbol{A}^{-\rm T}\boldsymbol{n}_{\rm tap}(i)\end{aligned} \tag{5b}$$

$$\boldsymbol{p}(i) = \boldsymbol{p}_{\rm inv}(i) - \boldsymbol{p}_{\rm l}(i) \tag{5c}$$

$$\boldsymbol{q}(i) = \boldsymbol{q}_{\rm inv}(i) + \boldsymbol{q}_{\rm c}(i) - \boldsymbol{q}_{\rm l}(i) \tag{5d}$$

$$\underline{\boldsymbol{v}} \leqslant \boldsymbol{v}(i) \leqslant \overline{\boldsymbol{v}} \tag{5e}$$

$$\underline{\boldsymbol{n}}_{\rm tap} \leqslant \boldsymbol{n}_{\rm tap}(i) \leqslant \overline{\boldsymbol{n}}_{\rm tap} \tag{5f}$$

$$\Delta\underline{\boldsymbol{n}}_{\rm tap} \leqslant \boldsymbol{n}_{\rm tap}(i) - \boldsymbol{n}_{\rm tap}(i-1) \leqslant \Delta\overline{\boldsymbol{n}}_{\rm tap} \tag{5g}$$

$$\boldsymbol{q}_{\rm c}(i) = \boldsymbol{n}_{\rm c}(i)\Delta q_{\rm c} \tag{5h}$$

$$0 \leqslant \boldsymbol{n}_{\rm c}(i) \leqslant \overline{\boldsymbol{n}}_{\rm c} \tag{5i}$$

$$\Delta\underline{\boldsymbol{n}}_{\rm c} \leqslant \boldsymbol{n}_{\rm c}(i) - \boldsymbol{n}_{\rm c}(i-1) \leqslant \Delta\overline{\boldsymbol{n}}_{\rm c} \tag{5j}$$

$$-\underline{\boldsymbol{q}}_{\rm inv}(i) = \overline{\boldsymbol{q}}_{\rm inv}(i) = \sqrt{{\rm S}_{\rm inv}(i)^2 - \boldsymbol{p}_{\rm inv}(i)^2} \tag{5k}$$

$$\underline{\boldsymbol{q}}_{\rm inv}(i) \leqslant \boldsymbol{q}_{\rm inv}(i) \leqslant \overline{\boldsymbol{q}}_{\rm inv}(i) \tag{5l}$$

where (5b)–(5d) represent DN power flow constraints, (5e) is the voltage upper/lower limit constraint, (5f)–(5g) and (5h)–(5j) represent the operation constraints for OLTC and CBs, respectively. (5k)–(5l) are the reactive power constraints for DG inverters.

B. Lower Stage Controller

The main objective of lower stage controller (LSC) is to remove instantaneous voltage violations. In this study, the active power output of DGs is assumed to follow maximum power point tracking (MPPT) mode [23] to capture the maximum active power and thus not controlled by LSC. LSC receives tap positions of OLTC $\boldsymbol{n}_{\rm tap}(T)$ and CBs $\boldsymbol{n}_{\rm c}(T)$ from USC, and dispatches the reactive power output of DG inverters. The adjustment of node reactive power injection has influence on network power losses [20], so the objective of LSC is to minimize the power losses. The LSC optimization problem at time instant t is formulated as:

$$\min_{\boldsymbol{q}_{\rm inv}} f(\boldsymbol{q}) = \frac{1}{2}\boldsymbol{q}(t)^{\rm T}\boldsymbol{X}\boldsymbol{q}(t) \tag{6a}$$

subject to

$$\begin{aligned}\boldsymbol{v}(t) = \boldsymbol{R}\boldsymbol{p}(t) + \boldsymbol{X}\boldsymbol{q}(t) + v_0\mathbf{1}_N \\ - 2v_{\rm nom}\Delta{\rm tap}\boldsymbol{A}^{-\rm T}\boldsymbol{n}_{\rm tap}(T)\end{aligned} \tag{6b}$$

$$\boldsymbol{p}(t) = \boldsymbol{p}_{\rm inv}(t) - \boldsymbol{p}_{\rm l}(t) \tag{6c}$$

$$\boldsymbol{q}(t) = \boldsymbol{q}_{\rm inv}(t) + \boldsymbol{q}_{\rm c}(t) - \boldsymbol{q}_{\rm l}(t) \tag{6d}$$

$$\underline{\boldsymbol{v}} \leqslant \boldsymbol{v}(t) \leqslant \overline{\boldsymbol{v}} \tag{6e}$$

$$\boldsymbol{q}_{\rm c}(t) = \boldsymbol{n}_{\rm c}(T)\Delta q_{\rm c} \tag{6f}$$

$$-\underline{\boldsymbol{q}}_{\rm inv}(t) = \overline{\boldsymbol{q}}_{\rm inv}(t) = \sqrt{{\rm S}_{\rm inv}(t)^2 - \boldsymbol{p}_{\rm inv}(t)^2} \tag{6g}$$

$$\underline{\boldsymbol{q}}_{\rm inv}(t) \leqslant \boldsymbol{q}_{\rm inv}(t) \leqslant \overline{\boldsymbol{q}}_{\rm inv}(t) \tag{6h}$$

where (6b)–(6d) represent the DN power flow constraints, (6e) denotes the voltage upper/lower limit constraint, (6f) represents the CB operation at time instant t while the reactive power constraints for DG inverters are described in (6g)–(6h).

Note that (6a) is not the exact power losses, but the equivalent power losses. The exact power losses can be given as:

$$P_{\rm loss} = \sum_{(i,j)\in\mathcal{L}} r_{ij}\frac{P_{ij}^2 + Q_{ij}^2}{v_0} \tag{7}$$

which can be expressed in compact form as:

$$P_{\rm loss} = \frac{1}{v_0}[(\boldsymbol{A}^{-1}\boldsymbol{p})^{\rm T}\boldsymbol{D}_r\boldsymbol{A}^{-1}\boldsymbol{p} + (\boldsymbol{A}^{-1}\boldsymbol{q})^{\rm T}\boldsymbol{D}_r\boldsymbol{A}^{-1}\boldsymbol{q}] \tag{8}$$

The active power output of DGs is assumed to be uncontrollable. So, minimizing power losses is equivalent to minimizing the second term in (8). Usually, distribution grid has homogeneous R/X ratio in practice, e.g. there exist a constant κ such that $r_{ij}/x_{ij} = \kappa, (i,j) \in \mathcal{L}$ [24], [25], the second term in (8) can be expressed as:

$$\begin{aligned}g(\boldsymbol{q}) &= \boldsymbol{q}^{\rm T}\boldsymbol{A}^{-\rm T}\boldsymbol{D}_r\boldsymbol{A}^{-1}\boldsymbol{q} \\ &\approx \kappa\boldsymbol{q}^{\rm T}\boldsymbol{A}^{-\rm T}\boldsymbol{D}_x\boldsymbol{A}^{-1}\boldsymbol{q} = \kappa\frac{1}{2}\boldsymbol{q}^{\rm T}\boldsymbol{X}\boldsymbol{q}\end{aligned} \tag{9}$$

Therefore, minimizing power losses is equivalent to the problem in (6) [19]. The reason for minimizing (6) instead of the exact power losses is to facilitate the implementation of the proposed distributed online voltage control, as demonstrated in the next section.

The lower stage problem (6) is in a centralized form. The main goal of the proposed TDO-VC is to design a distributed online voltage control framework relying on communication with physical connected neighbouring buses, so the distributed realization of (6) will be introduced in the following section.

IV. Distributed Online Voltage Control Design

In this section, the proposed distributed framework as well as the theoretical basis behind the controller design is introduced. In addition, the convergence and computation analysis on the proposed method are provided.

A. Dual Problem

The Lagrangian function of problem (6) is given as:

$$\begin{aligned}\mathcal{L}(\boldsymbol{q},\boldsymbol{\nu}) = \frac{1}{2}\boldsymbol{q}^{\rm T}\boldsymbol{X}\boldsymbol{q} + \overline{\boldsymbol{\mu}}^{\rm T}(\boldsymbol{v}-\overline{\boldsymbol{v}}) + \underline{\boldsymbol{\mu}}^{\rm T}(\underline{\boldsymbol{v}}-\boldsymbol{v}) \\ + \overline{\boldsymbol{\lambda}}^{\rm T}(\boldsymbol{q}-\overline{\boldsymbol{q}}) + \underline{\boldsymbol{\lambda}}^{\rm T}(\underline{\boldsymbol{q}}-\boldsymbol{q})\end{aligned} \tag{10}$$

For brevity, the notation of time instant t is omitted, and (10) can be further reorganized into a compact form as follows:

$$\mathcal{L}(\boldsymbol{q},\boldsymbol{\nu}) = \frac{1}{2}\boldsymbol{q}^{\mathrm{T}}\boldsymbol{X}\boldsymbol{q} + \boldsymbol{\nu}^{\mathrm{T}}(\boldsymbol{M}\boldsymbol{q}+\boldsymbol{c}) \tag{11}$$

where

$$\boldsymbol{\nu} = \begin{bmatrix} \overline{\boldsymbol{\mu}} \\ \underline{\boldsymbol{\mu}} \\ \overline{\boldsymbol{\lambda}} \\ \underline{\boldsymbol{\lambda}} \end{bmatrix},\ \boldsymbol{M} = \begin{bmatrix} \boldsymbol{X} \\ -\boldsymbol{X} \\ \boldsymbol{I}_N \\ -\boldsymbol{I}_N \end{bmatrix},\ \boldsymbol{c} = \begin{bmatrix} \boldsymbol{v}_{\mathrm{un}} - \overline{\boldsymbol{v}} \\ -\boldsymbol{v}_{\mathrm{un}} + \underline{\boldsymbol{v}} \\ \boldsymbol{0}_N \\ \boldsymbol{0}_N \end{bmatrix}$$

Here, $\boldsymbol{v}_{\mathrm{un}} = \boldsymbol{R}\boldsymbol{p} + v_0\boldsymbol{1}_N - 2v_{\mathrm{nom}}\Delta\mathrm{tap}\boldsymbol{A}^{-\mathrm{T}}\boldsymbol{n}_{\mathrm{tap}}$ represents the uncontrollable terms in the lower stage.

By setting $\nabla_{\boldsymbol{q}}\mathcal{L} = 0$ we have

$$\boldsymbol{q} = -\boldsymbol{B}\boldsymbol{M}^{\mathrm{T}}\boldsymbol{\nu} \tag{12}$$

where $\boldsymbol{B} = \boldsymbol{X}^{-1}$ is the weighted Laplacian matrix. Then the dual function is given as:

$$d(\boldsymbol{\nu}) := \inf\mathcal{L}(\boldsymbol{q},\boldsymbol{\nu}) = -\frac{1}{2}\boldsymbol{\nu}^{\mathrm{T}}\boldsymbol{M}\boldsymbol{B}\boldsymbol{M}^{\mathrm{T}}\boldsymbol{\nu} + \boldsymbol{\nu}^{\mathrm{T}}\boldsymbol{c} \tag{13}$$

The dual problem (D) of lower stage control is given as:

$$\max_{\boldsymbol{\nu}\geqslant 0} d(\boldsymbol{\nu}) \tag{14}$$

The problem (D) can be solved by DA [10], [20]. However, the shortcomings with DA is that its convergence rate is slow. The convergence speed is an important factor that needs to be considered for online voltage control, so Gf-DA with fast convergence rate is applied to solve problem (D) efficiently.

B. Generalized Fast Dual Ascent

Given the fact f is strictly convex and the constraint is convex, d is concave and differentiable with gradient

$$\nabla d(\boldsymbol{\nu}) = -\boldsymbol{M}\boldsymbol{B}\boldsymbol{M}^{\mathrm{T}}\boldsymbol{\nu} + \boldsymbol{c} \tag{15}$$

we have

$$\|-\nabla d(\boldsymbol{\nu}_1) + \nabla d(\boldsymbol{\nu}_2)\|_2 \leqslant \|\boldsymbol{M}\boldsymbol{B}\boldsymbol{M}^{\mathrm{T}}\|_2\|\boldsymbol{\nu}_1 - \boldsymbol{\nu}_2\|_2 \tag{16}$$

holds for all $\boldsymbol{\nu}_1, \boldsymbol{\nu}_2 \in \mathbb{R}^{4N}$, which indicates -$d$ has a Lipschitz continous gradient with constant $L = \|\boldsymbol{M}\boldsymbol{B}\boldsymbol{M}^{\mathrm{T}}\|_2$.

By generalizing the Lipschitz constant L, (16) can be adapted into its generalized counterpart [26]

$$d(\boldsymbol{\nu}_1) \geqslant d(\boldsymbol{\nu}_2) + \nabla d(\boldsymbol{\nu}_2)^{\mathrm{T}}(\boldsymbol{\nu}_1 - \boldsymbol{\nu}_2) - \frac{1}{2}\|\boldsymbol{\nu}_1 - \boldsymbol{\nu}_2\|_{\boldsymbol{L}}^2 \tag{17}$$

where $\|\boldsymbol{x}\|_{\boldsymbol{L}} = \sqrt{\boldsymbol{x}^{\mathrm{T}}\boldsymbol{L}\boldsymbol{x}}$, which holds for all $\boldsymbol{\nu}_1, \boldsymbol{\nu}_2$, any $\boldsymbol{L} \in \mathbb{R}^{4N\times 4N}$ is positive definite and satisfy $\boldsymbol{L} \succeq \boldsymbol{M}\boldsymbol{B}\boldsymbol{M}^{\mathrm{T}}$.

The right hand side in (17) actually gives a quadratic lower bound of problem (D). The basic idea of Gf-DA is to maximize this lower bound, instead of the original dual function. In addition, the generalization of matrix $\boldsymbol{L}$ allows for lower bound with different curvature in different directions, which consequently achieve improved convergence rate. The Gf-DA algorithm for problem (D) is summarized in Algorithm 1.

Algorithm 1: Gf-DA for problem (D)

Initialization: $\boldsymbol{\varepsilon}^1 = \boldsymbol{\nu}^0, \gamma^1 = 1$, where $\boldsymbol{\varepsilon} = \left[\overline{\boldsymbol{\omega}}^{\mathrm{T}}, \underline{\boldsymbol{\omega}}^{\mathrm{T}}, \overline{\boldsymbol{\eta}}^{\mathrm{T}}, \underline{\boldsymbol{\eta}}^{\mathrm{T}}\right]^{\mathrm{T}}$

for $k \geqslant 1$ **do**

Update primal variable

$$\begin{aligned}\text{Step 1:}\boldsymbol{q}^k &= \operatorname*{argmin}_{\boldsymbol{q}}\ \mathcal{L}\left(\boldsymbol{q}, \boldsymbol{\nu}^{k-1}\right)\\ &= -\boldsymbol{B}\boldsymbol{M}^{\mathrm{T}}\boldsymbol{\nu}^{k-1}\end{aligned}$$

Update dual variable

$$\text{Step 2:}\begin{cases} \overline{\boldsymbol{\mu}}^k \leftarrow [\overline{\boldsymbol{\omega}}^k + [\boldsymbol{L}^{-1}]_{\overline{\boldsymbol{\mu}}}\nabla_{\overline{\boldsymbol{\mu}}}d(\boldsymbol{\nu})]^+ \\ \underline{\boldsymbol{\mu}}^k \leftarrow [\underline{\boldsymbol{\omega}}^k + [\boldsymbol{L}^{-1}]_{\underline{\boldsymbol{\mu}}}\nabla_{\underline{\boldsymbol{\mu}}}d(\boldsymbol{\nu})]^+ \\ \overline{\boldsymbol{\lambda}}^k \leftarrow [\overline{\boldsymbol{\eta}}^k + [\boldsymbol{L}^{-1}]_{\overline{\lambda}}\nabla_{\overline{\lambda}}d(\boldsymbol{\nu})]^+ \\ \underline{\boldsymbol{\lambda}}^k \leftarrow [\underline{\boldsymbol{\eta}}^k + [\boldsymbol{L}^{-1}]_{\underline{\lambda}}\nabla_{\underline{\lambda}}d(\boldsymbol{\nu})]^+ \end{cases}$$

$$\text{Step 3:}\ \gamma^{k+1} \leftarrow \frac{1+\sqrt{1+4(\gamma^k)^2}}{2},\ \varphi^k = \frac{\gamma^k - 1}{\gamma^{k+1}}$$

$$\text{Step 4:}\begin{cases} \overline{\boldsymbol{\omega}}^{k+1} \leftarrow \overline{\boldsymbol{\mu}}^k + \varphi^k(\overline{\boldsymbol{\mu}}^k - \overline{\boldsymbol{\mu}}^{k-1}) \\ \underline{\boldsymbol{\omega}}^{k+1} \leftarrow \underline{\boldsymbol{\mu}}^k + \varphi^k(\underline{\boldsymbol{\mu}}^k - \underline{\boldsymbol{\mu}}^{k-1}) \\ \overline{\boldsymbol{\eta}}^{k+1} \leftarrow \overline{\boldsymbol{\lambda}}^k + \varphi^k(\overline{\boldsymbol{\lambda}}^k - \overline{\boldsymbol{\lambda}}^{k-1}) \\ \underline{\boldsymbol{\eta}}^{k+1} \leftarrow \underline{\boldsymbol{\lambda}}^k + \varphi^k(\underline{\boldsymbol{\lambda}}^k - \underline{\boldsymbol{\lambda}}^{k-1}) \end{cases}$$

end

where $[\cdot]^+$ denotes the projection operator onto the non-negative range. $[\boldsymbol{L}^{-1}]_{\nu_i}$, $\boldsymbol{\nu}_i \in \bar{\boldsymbol{\mu}}$, $\underline{\boldsymbol{\mu}}$, $\overline{\boldsymbol{\lambda}}$, $\underline{\boldsymbol{\lambda}}$ represents the submatrix of $[\boldsymbol{L}^{-1}]$ accociated with each dual variable vector.

C. Distributed Implementation

Algorithm 1 is calculated in a centralized way, and the distributed solution of Algorithm 1 is derived in this section. The Lagrangian function (10) is rewritten in distributed form

$$\begin{aligned}\mathcal{L}(\boldsymbol{q},\boldsymbol{\nu}) = \sum_{i=1}^{N} & f_i(q_i) + \overline{\mu}_i(v_i - \overline{v}) + \underline{\mu}_i(\underline{v} - v_i) \\ & + \overline{\lambda}_i(q_i - \overline{q}) + \underline{\lambda}_i(\underline{q} - q_i)\end{aligned} \tag{18}$$

1) Primal Update

To derive distributed solution of primal update of Step 1 in Algorithm 1, Proposition 1 is given here.

Proposition 1. The structure of weighted Laplacian matrix $\boldsymbol{B}$ is sparse and determined by the topology of physical electrical network. For any pair of buses (i, j) that are not directly connected, the corresponding entry of $\boldsymbol{B}$ is zero, i.e., $B_{ij} = 0,\ \forall(i,j) \notin \mathcal{L}$.

Proof. By definition, $\boldsymbol{B} := (1/2)\boldsymbol{A}\boldsymbol{D}_x^{-1}\boldsymbol{A}^{\mathrm{T}} = [B_{ij}] \in \mathbb{R}^{N\times N}$, we have

$$B_{ij} = \frac{1}{2}\sum_{l=1}^{N}\boldsymbol{A}_{il}\boldsymbol{D}_{x,ll}^{-1}\boldsymbol{A}_{jl}$$

According the definition of $\boldsymbol{A}$, $\boldsymbol{A}_{il}\boldsymbol{A}_{jl} = 0$ if bus i and bus j are not connected, thus $B_{ij} = 0$.

Substituting $\boldsymbol{M}$ and $\boldsymbol{\nu}$ into (12) and considering that $\boldsymbol{X}$ is symmetric, we have the primal update in a centralized form as follows:

$$\boldsymbol{q} = -\overline{\boldsymbol{\mu}} + \underline{\boldsymbol{\mu}} - \boldsymbol{B}\overline{\boldsymbol{\lambda}} + \boldsymbol{B}\underline{\boldsymbol{\lambda}} \tag{19}$$

So, the reactive power value at bus i obtained by primal update is the i_th element in $\boldsymbol{q}$.

$$q_i^* = -\overline{\mu}_i + \underline{\mu}_i + \sum_{j=1}^{N} B_{ij}(\underline{\lambda}_j - \overline{\lambda}_j) \tag{20}$$

According to Proposition 1, $B_{ij} = 0$ if bus i and bus j are not physical connected. Thus, (20) can be equivalently given as:

$$q_i^* = -\overline{\mu}_i + \underline{\mu}_i + \sum_{j\in\mathcal{N}_i} B_{ij}(\underline{\lambda}_j - \overline{\lambda}_j) \tag{21}$$

In (21), the update of primal variable at each bus i only involves information of itself and physical directly connected neighbouring buses. In this way, the primal update can be implemented in a fully distributed way.

The reactive power limit is relaxed in primal update, which might lead to infeasible point. Hence, the reactive power setpoint at each bus i should be projected to feasible range

$$q_i = [q_i^*]_{\underline{q}_i}^{\overline{q}_i} \tag{22}$$

where $[\cdot]_a^b$ is the projection operator onto the range $[a, b]$.

2) Dual Update

As can be seen from (18), the gradient of dual function is naturally decomposable,

$$\nabla_{\overline{\mu}_i} d(\boldsymbol{\nu}) = v_i - \overline{v}_i,\ \nabla_{\underline{\mu}_i} d(\boldsymbol{\nu}) = \underline{v}_i - v_i \tag{23a}$$

$$\nabla_{\overline{\lambda}_i} d(\boldsymbol{\nu}) = q_i - \overline{q}_i,\ \nabla_{\underline{\lambda}_i} d(\boldsymbol{\nu}) = \underline{q}_i - q_i \tag{23b}$$

The last step is to choose matrix $\boldsymbol{L}$ in order to facilitate a distributed design of dual update. One intuitive way is to choose a block diagonal matrix, e.g. $\boldsymbol{L} = \text{blkdiag}(\boldsymbol{L}_{\overline{\mu}}, \boldsymbol{L}_{\underline{\mu}}, \boldsymbol{L}_{\overline{\lambda}}, \boldsymbol{L}_{\underline{\lambda}})$. In addition, to guarantee the algorithm convergence, $\boldsymbol{L}$ should satisfy $\boldsymbol{L} \succeq \boldsymbol{MBM}^{\mathrm{T}}$. Then, $\boldsymbol{L}$ can be determined by solving the following semi-definite programming problem,

$$\min_{\boldsymbol{L}} \ \text{Trace}(\boldsymbol{L}) \tag{24a}$$

$$\text{s.t. } \boldsymbol{L} \succeq \boldsymbol{MBM}^{\mathrm{T}} \tag{24b}$$

where $\boldsymbol{L}$ can be calculated offline one time and keeps fixed during the whole control period. Each element $\boldsymbol{L}_i$ associated with bus i will be stored in its control unit. After $\boldsymbol{L}$ is determined, the dual update for $\overline{\mu}_i$ in Step 2 can be fully decomposed as:

$$\overline{\mu}_i^k \leftarrow \overline{\omega}_i^k + (v_i^k - \overline{v})/L_{\overline{\mu}_i} \tag{25}$$

where $\underline{\mu}_i$, $\overline{\lambda}_i$ and $\underline{\lambda}_i$ can be updated in similar way.

The online distributed voltage control algorithm for each bus i is described in Algorithm 2. In Algorithm 2, the reactive power setpoint at each bus can be updated online based on information of itself and physical connected neighbouring buses. No centralized control is needed and the communication complexity can be significantly reduced.

D. Convergence and Computation Analysis

To compare the convergence rate between the proposed TDO-VC and conventional gradient methods, two propositions are provided here.

Algorithm 2: Online Distributed Voltage Control

Initialization: $\varepsilon_i^1 = v_i^0, \gamma^1 = 1$

for $k \geqslant 1$ **do**

Measurement: Measure bus voltage magnitude and get v_i

Information exchange: Send $\underline{\lambda}_i^k, \overline{\lambda}_i^k$ to neighbouring buses j and receive $\underline{\lambda}_j^k, \overline{\lambda}_j^k$ from j, $j \in \mathcal{N}_i$

Update primal variable

$$q_i^k = \underline{\mu}_i^{k-1} - \overline{\mu}_i^{k-1} + \sum_{j\in\mathcal{N}_i} B_{ij}(\underline{\lambda}_j^{k-1} - \overline{\lambda}_j^{k-1})$$

Update dual variable

$$\text{Step 2: } \begin{cases} \overline{\mu}_i^k \leftarrow [\overline{\omega}_i^k + (v_i^k - \overline{v})/L_{\overline{\mu}_i}]^+ \\ \underline{\mu}_i^k \leftarrow [\underline{\omega}_i^k + (\underline{v} - v_i^k)/L_{\underline{\mu}_i}]^+ \\ \overline{\lambda}_i^k \leftarrow [\overline{\eta}_i^k + (q_i^k - \overline{q}_i)/L_{\overline{\lambda}_i}]^+ \\ \underline{\lambda}_i^k \leftarrow [\underline{\eta}_i^k + (\underline{q}_i - q_i^k)/L_{\underline{\lambda}_i}]^+ \end{cases}$$

$$\text{Step 3: } \gamma^{k+1} \leftarrow \frac{1+\sqrt{1+4(\gamma^k)^2}}{2},\ \varphi^k = \frac{\gamma^k - 1}{\gamma^{k+1}}$$

$$\text{Step 4: } \begin{cases} \overline{\omega}_i^{k+1} \leftarrow \overline{\mu}_i^k + \varphi^k(\overline{\mu}_i^k - \overline{\mu}_i^{k-1}) \\ \underline{\omega}_i^{k+1} \leftarrow \underline{\mu}_i^k + \varphi^k(\underline{\mu}_i^k - \underline{\mu}_i^{k-1}) \\ \overline{\eta}_i^{k+1} \leftarrow \overline{\lambda}_i^k + \varphi^k(\overline{\lambda}_i^k - \overline{\lambda}_i^{k-1}) \\ \underline{\eta}_i^{k+1} \leftarrow \underline{\lambda}_i^k + \varphi^k(\underline{\lambda}_i^k - \underline{\lambda}_i^{k-1}) \end{cases}$$

Implement: Apply the reactive power setpoint $q_i = \left[q_i^k\right]_{\underline{q}_i}^{\overline{q}_i}$

end

Proposition 2. If the step size in DA is chosen as $\alpha \in (0, 1/L]$, then the algorithm converges with rate,

$$d(\boldsymbol{\nu}^*) - d(\boldsymbol{\nu}^k) \leqslant \frac{\|\boldsymbol{\nu}^* - \boldsymbol{\nu}^0\|_2^2}{2\alpha k} \tag{26}$$

Proposition 3. Suppose $\boldsymbol{L} = \text{blkdiag}(\boldsymbol{L}_{\overline{\mu}}, \boldsymbol{L}_{\underline{\mu}}, \boldsymbol{L}_{\overline{\lambda}}, \boldsymbol{L}_{\underline{\lambda}})$ which is positive definite and satisfy $\boldsymbol{L} \succeq \boldsymbol{MBM}^{\mathrm{T}}$, the Gf-DA algorithm converges with rate,

$$d(\boldsymbol{\nu}^*) - d(\boldsymbol{\nu}^k) \leqslant \frac{2\|\boldsymbol{\nu}^* - \boldsymbol{\nu}^0\|_{\boldsymbol{L}}^2}{(k+1)^2} \tag{27}$$

Detailed proof is included in the Appendix. From Propositions 2 and 3, we know that DA solves the problem with convergence rate $O(1/k)$ while the Gf-DA can achieve an improved convergence rate no worse than $O(1/k^2)$. It means that the proposed TDO-VC can significantly accelerate the solution speed and it is more suitable for online control.

E. Extension to Unbalanced Distribution Network

To extend the proposed TDO-VC to unbalanced DN, firstly the linear Distflow model for multi-phase DN is introduced. Without loss of generality, each bus or branch is assumed to have all three phases, yet represented by a 3×1 complex vector. For each bus $i \in \mathcal{N}$, let $\tilde{\boldsymbol{V}}_i := [V_i^a \ \ V_i^b \ \ V_i^c]^{\mathrm{T}}$ denote the three-phase voltages. For each branch $(i, j) \in \mathcal{L}$, let $\tilde{\boldsymbol{I}}_{ij} := [I_{ij}^a \ \ I_{ij}^b \ \ I_{ij}^c]^{\mathrm{T}}$ and $\tilde{\boldsymbol{S}}_{ij} := [S_{ij}^a \ \ S_{ij}^b \ \ S_{ij}^c]^{\mathrm{T}}$ denote its three-phase line current and complex power flow, respectively.

The multi-phase power flow equation for each branch including OLTC tap ratio $\tilde{t}_{\text{tap},ij}$ is governed by Ohm's law,

$$\tilde{\boldsymbol{S}}_{ij} - \tilde{\boldsymbol{z}}_{ij}\tilde{\boldsymbol{I}}_{ij} \odot \tilde{\boldsymbol{I}}_{ij}^{*} - \sum_{k\in\mathcal{C}_j} \tilde{\boldsymbol{S}}_{ij} = -\tilde{\boldsymbol{s}}_j \tag{28a}$$

$$\tilde{\boldsymbol{t}}_{\text{tap},ij} \odot \tilde{\boldsymbol{V}}_i - \tilde{\boldsymbol{z}}_{ij}\tilde{\boldsymbol{I}}_{ij} = \tilde{\boldsymbol{V}}_j \tag{28b}$$

where $\tilde{\boldsymbol{z}}_{ij} := \tilde{\boldsymbol{r}}_{ij} + j\tilde{\boldsymbol{x}}_{ij} \in \mathbb{C}^{3\times 3}$ is 3×3 full symmetric impedance matrix of branch (i,j) and $\tilde{\boldsymbol{t}}_{\text{tap},ij} = 1 + \tilde{\boldsymbol{n}}_{\text{tap},ij}\,\Delta\text{tap}_{ij}$ with $\tilde{\boldsymbol{n}}_{\text{tap},ij}$ is three-phase OLTC tap position and Δtap_{ij} is OLTC voltage change per step. $\odot$ denotes the element-wise multiplication.

Given the fact that voltage magnitudes between phases are similar, we have $\tilde{V}_i \approx |V_i|\boldsymbol{\alpha}$, $\boldsymbol{\alpha} := [1 \;\; \alpha \;\; \alpha^2]^{\mathrm{T}}$, $\alpha = e^{-j(2\pi/3)}$ [27]. The multi-phase linear Distflow model can be derived as [22], [28],

$$\tilde{\boldsymbol{P}}_{ij} - \sum_{k\in\mathcal{C}_j} \tilde{\boldsymbol{P}}_{jk} = -\tilde{\boldsymbol{p}}_j \tag{29a}$$

$$\tilde{\boldsymbol{Q}}_{ij} - \sum_{k\in\mathcal{C}_j} \tilde{\boldsymbol{Q}}_{jk} = -\tilde{\boldsymbol{q}}_j \tag{29b}$$

$$\tilde{\boldsymbol{v}}_i - \tilde{\boldsymbol{v}}_j = 2(\hat{\boldsymbol{r}}_{ij}\tilde{\boldsymbol{P}}_{ij} + \hat{\boldsymbol{x}}_{ij}\tilde{\boldsymbol{Q}}_{ij}) - 2\tilde{\boldsymbol{n}}_{\text{tap},ij}\Delta\text{tap}_{ij}v_{\text{nom}} \tag{29c}$$

where $\tilde{\boldsymbol{v}}_i := [|V_i^a|^2 \;\; |V_i^b|^2 \;\; |V_i^c|^2]^{\mathrm{T}}$ represents the three-phase squared voltage magnitude at bus i and $\hat{\boldsymbol{z}}_{ij} = \hat{\boldsymbol{r}}_{ij} + \boldsymbol{i}\hat{\boldsymbol{x}}_{ij} = [(\boldsymbol{\alpha}\boldsymbol{\alpha}^{\mathrm{H}}) \odot \tilde{\boldsymbol{z}}_{ij}^{*}]^{*}$.

To compact form of linear Distflow model can be extended into multi-phase representation by extending the incidence matrix $\bar{\boldsymbol{A}}$ into $\tilde{\boldsymbol{A}} := \overline{\boldsymbol{A}} \otimes \boldsymbol{I}_3$. Then the compact form representation of multi-phase linear Distflow can be expressed as:

$$-\tilde{\boldsymbol{A}}\tilde{\boldsymbol{P}} = -\tilde{\boldsymbol{p}} \tag{30a}$$

$$-\tilde{\boldsymbol{A}}\tilde{\boldsymbol{Q}} = -\tilde{\boldsymbol{q}} \tag{30b}$$

$$\tilde{\boldsymbol{v}} = \tilde{\boldsymbol{R}}\tilde{\boldsymbol{p}} + \tilde{\boldsymbol{X}}\tilde{\boldsymbol{q}} + v_0\boldsymbol{1}_{3N} - 2v_{\text{nom}}\Delta\text{tap}\tilde{\boldsymbol{A}}^{-\mathrm{T}}\tilde{\boldsymbol{n}}_{\text{tap}} \tag{30c}$$

where $\tilde{\boldsymbol{R}} = 2\tilde{\boldsymbol{A}}^{-\mathrm{T}}\text{blkdiag}[\hat{\boldsymbol{r}}_i]\tilde{\boldsymbol{A}}^{-1}$ and $\tilde{\boldsymbol{X}} = 2\tilde{\boldsymbol{A}}^{-\mathrm{T}}\text{blkdiag}[\hat{\boldsymbol{x}}_i]\tilde{\boldsymbol{A}}^{-1}$, $\hat{\boldsymbol{r}}_i$ and $\hat{\boldsymbol{x}}_i$ are the i_th element of $\hat{\boldsymbol{r}}_{ij}$ and $\hat{\boldsymbol{x}}_{ij} \in \mathcal{L}$, respectively.

Then, the upper stage optimization problem can be obtained by extending (5) into three-phase representation accordingly. Similarly, the objective functions of the lower stage problem (6a) can be extended as:

$$\min_{\tilde{\boldsymbol{q}}_{\text{inv}}} f(\tilde{\boldsymbol{q}}) = \frac{1}{2}\tilde{\boldsymbol{q}}^{\mathrm{T}}\tilde{\boldsymbol{X}}\tilde{\boldsymbol{q}} \tag{31}$$

The Lagrangian function of the lower stage problem can be expressed as:

$$\begin{aligned}\mathcal{L}(\tilde{\boldsymbol{q}},\tilde{\boldsymbol{\nu}}) = \frac{1}{2}\tilde{\boldsymbol{q}}^{\mathrm{T}}\tilde{\boldsymbol{X}}\tilde{\boldsymbol{q}} + \overline{\boldsymbol{\mu}}^{\mathrm{T}}(\tilde{\boldsymbol{v}} - \overline{\boldsymbol{v}}) + \underline{\boldsymbol{\mu}}^{\mathrm{T}}(\underline{\boldsymbol{v}} - \tilde{\boldsymbol{v}}) \\ + \overline{\boldsymbol{\lambda}}^{\mathrm{T}}(\tilde{\boldsymbol{q}} - \overline{\boldsymbol{q}}) + \underline{\boldsymbol{\lambda}}^{\mathrm{T}}(\underline{\boldsymbol{q}} - \tilde{\boldsymbol{q}})\end{aligned} \tag{32}$$

The close-form solution for the primal update can be obtained following (12):

$$\tilde{\boldsymbol{q}} = -\tilde{\boldsymbol{B}}\tilde{\boldsymbol{M}}^{\mathrm{T}}\tilde{\boldsymbol{\nu}} \tag{33}$$

where $\tilde{\boldsymbol{M}} = [\tilde{\boldsymbol{X}}^{\mathrm{T}} \;\; \tilde{\boldsymbol{X}}^{\mathrm{T}} \;\; \boldsymbol{I}_{3N} \;\; \boldsymbol{I}_{3N}]^{\mathrm{T}}$, $\tilde{\boldsymbol{B}} = -\tilde{\boldsymbol{X}}$, $\tilde{\boldsymbol{\nu}} \in \mathbb{R}^{12N}$ is the multi-phase extension of $\boldsymbol{\nu}$.

Proposition 4. The matrix $\tilde{\boldsymbol{B}}$ can be divided into $N \times N$ blocks with each block being a 3×3 square submatrix. For any pair of buses (i,j) that are not directly connected, the corresponding submatrix $\tilde{\boldsymbol{B}}_{ij}$ is a 3×3 zero matrix.

Proof. By definition,

$$\tilde{\boldsymbol{B}}_{ij} = (1/2)\sum_{l=1}^{N}(A_{il}\boldsymbol{I}_3)\hat{\boldsymbol{x}}_l^{-1}(A_{jl}\boldsymbol{I}_3) = (1/2)\sum_{l=1}^{N}A_{il}A_{jl}\hat{\boldsymbol{x}}_l^{-1}$$

According the definition of $\boldsymbol{A}$, $\boldsymbol{A}_{il}\boldsymbol{A}_{jl} = 0$ if bus i and bus j are not connected. Thus, the submatrix $\tilde{\boldsymbol{B}}_{ij}$ is a 3×3 zero matrix.

According to (32), the gradient of dual function can be expressed as:

$$\nabla_{\overline{\boldsymbol{\mu}}}d(\tilde{\boldsymbol{\nu}}) = \tilde{\boldsymbol{v}} - \overline{\boldsymbol{v}},\;\; \nabla_{\underline{\boldsymbol{\mu}}}d(\tilde{\boldsymbol{\nu}}) = \underline{\boldsymbol{v}} - \tilde{\boldsymbol{v}} \tag{34a}$$

$$\nabla_{\overline{\boldsymbol{\lambda}}}d(\tilde{\boldsymbol{\nu}}) = \tilde{\boldsymbol{q}} - \overline{\boldsymbol{q}},\;\; \nabla_{\underline{\boldsymbol{\lambda}}}d(\tilde{\boldsymbol{\nu}}) = \underline{\boldsymbol{q}} - \tilde{\boldsymbol{q}} \tag{34b}$$

which is naturally decomposable.

Following the logic of the derivation in Section IV-C, the update of primal variable at each bus i can be implemented by information exchange between physical directly connected neighbouring buses. Also, the gradient of the dual function of the multi-phase representation is naturally decomposable. By choosing a block diagonal matrix $\boldsymbol{L}$, the proposed TDO-VC can be implemented distributed online on unbalanced DN.

V. Case Study

In this section, the performance of the proposed method is verified on a modified balanced IEEE-123 bus system. Network parameters can be found in [29]. The daily minute-interval solar and load profiles are obtained from the National Renewable Energy Laboratory (NREL) Renewable Resource Data Center [30], as shown in Figs. 3 and 4. The location of OLTC transformers, CBs and DGs is described in Fig. 5. For each OLTC, the voltage regulation range is $\pm$ 5% with 20 tap

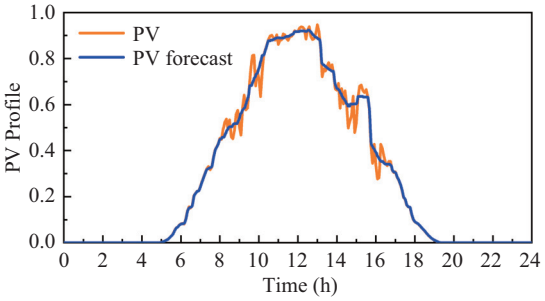

Fig. 3. PV profile.

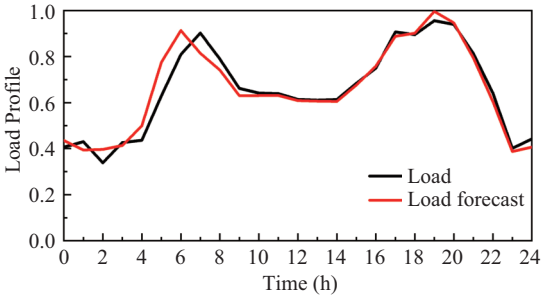

Fig. 4. Load profile.

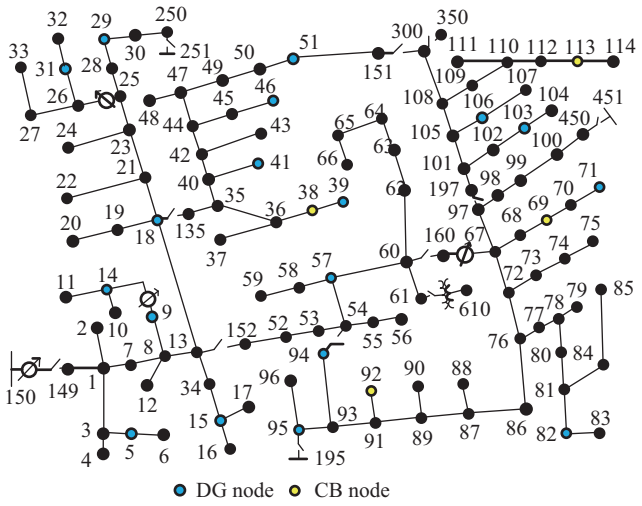

Fig. 5. IEEE-123 bus test feeder.

positions. The capacity of each CB is 300 kVar with 5 tap positions, and the capacity of each DG inverter is 800 kVA. All the simulations are performed in MATLAB r2021b on an ordinary computer running Win 10 with 3.9 GHz CPU and 32G RAM, and the upper stage optimization problem is solved by Gurobi solver [31].

A. Static Performance

The proposed TDO-VC is compared with other benchmark methods in terms of convergence rate and optimality. Two typical cases are selected: Case 1 at 12:00, when there is high PV generation and low load consumption; and Case 2 at 20:00, when there is low PV generation and high load demand.

The convergence analysis in Case 1 is illustrated in Fig. 6. Bus 94 with the maximum voltage magnitude is selected to illustrate the convergence of bus voltage. In addition, the convergence of the power losses is illustrated to compare the performance of the proposed method with other benchmark methods under snapshot static simulation. In addition, the simulation results in Case 1 are summarized in Table II. As can be seen from the simulation results, the conventional DA and ADMM [32] require a large number of iterations to converge. By contrast, the proposed TDO-VC can achieve a much faster convergence rate than the above two methods without sacrificing optimality. The proposed TDO-VC can reach the optimum point using 58 iterations, while DA and ADMM take 183 and 256 iterations, respectively. The computation time of the proposed TDO-VC is nearly half of that in DA and ADMM. Droop control can achieve the fastest convergence speed thanks to its simple updating rule. However, it suffers from degraded performance in power losses minimization due to its local nature. The steady state power losses in droop control are 1030 kW while for other methods are 975 kW. The simulation results in Case 2 are described in Fig. 7 and Table III. Bus 82 with the minimum voltage magnitude is chosen for demonstration in Case 2. The simulation results are quite similar to those in Case 1. The power losses obtained by droop control are 88 kW, which is 1.034 larger than that in other methods. Hence, the proposed TDO-VC can achieve better performance than other methods in terms of convergence rate and optimality.

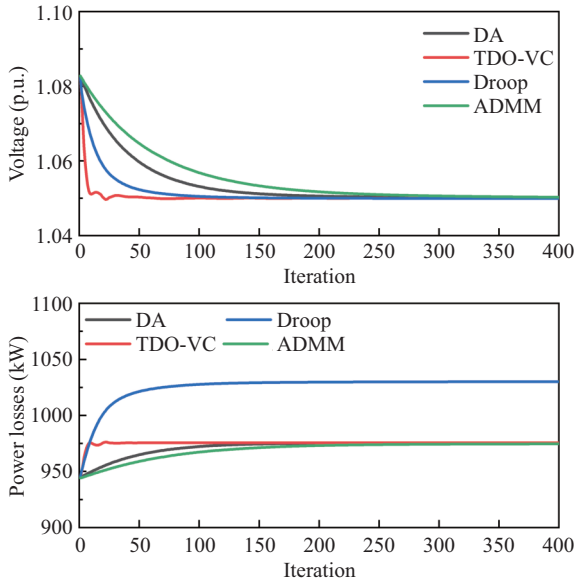

Fig. 6. Convergence analysis in Case 1.

TABLE II
COMPARISON OF SIMULATION RESULTS IN CASE 1

Description	DA	TDO-VC	Droop	ADMM
Convergence iterations	183	58	105	256
Computation time ($\times 10^{-3}$ s)	1.13	0.554	0.342	1.21

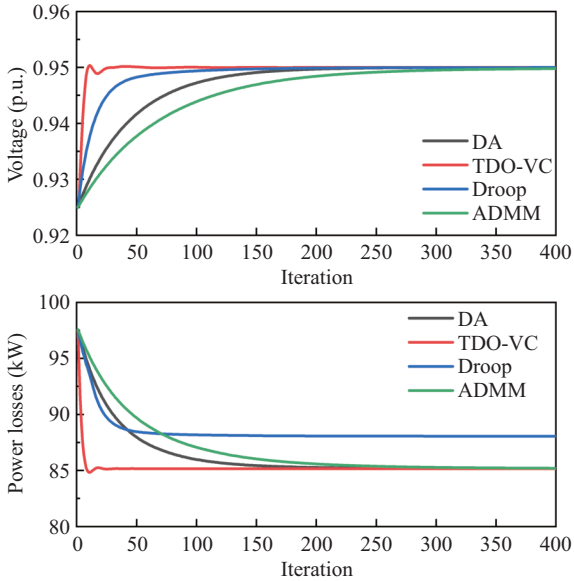

Fig. 7. Convergence analysis in Case 2.

TABLE III
COMPARISON OF SIMULATION RESULTS IN CASE 2

Description	DA	TDO-VC	Droop	ADMM
Convergence iterations	197	62	126	287
Computation time ($\times 10^{-3}$ s)	1.18	0.583	0.391	1.33

B. Robustness

In real practice, communication interruption may happen due to random communication delay or package drop. Because the updates of primal and dual variables depend on communications between neighbours, the robustness against potential communication failure needs to be verified. In this section, simulations under random communication failure possibilities ρ are performed. The freezing strategy, which was introduced in [33], is applied to facilitate the asynchronous implementation. In freezing strategy, the exchanged variables stay unchanged until there's new information coming from neighbouring node. The convergence results of bus voltages in two cases are illustrated in Figs. 8 and 9, respectively, where $\rho = 0$ represents the scenario without communication failure or delay. From Figs. 8 and 9 we can see, the proposed method performs well under different communication failure rates, showing high robustness to communication failures.

The proposed method is also tested against modeling errors in this section. The modeling errors are assumed to follow normal distribution with zero mean and different standard variations in this study. For both cases, the simulation is performed 1000 times to obtain the statistical results of the max/min bus voltage magnitudes in Case 1 and Case 2. The results are evaluated in three dimensions, the max/min observed voltages, the mean and standard deviations of the statistical results, in Tables IV and V, respectively. In both cases, the statical voltage magnitudes stay quite close to the voltage lower/upper bound, demonstrating that the proposed method is robust to modeling errors.

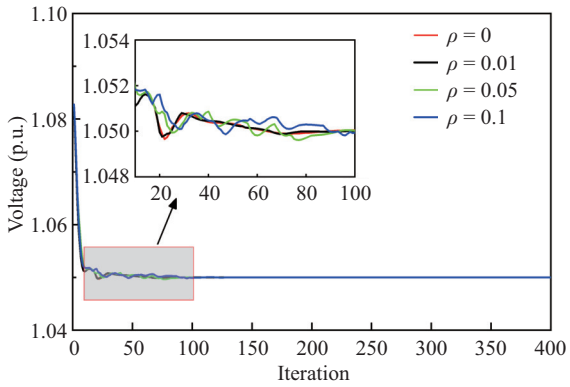

Fig. 8. Convergence in case 1 with asynchronous communication.

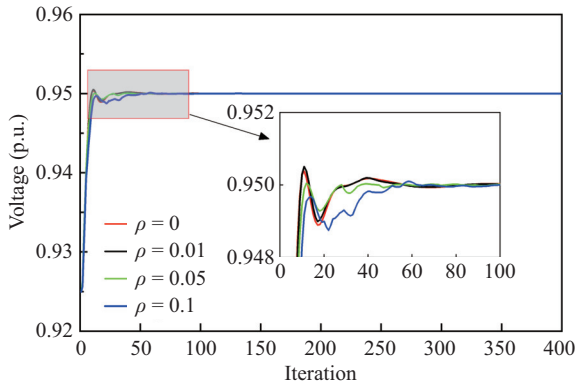

Fig. 9. Convergence in case 2 with asynchronous communication.

TABLE IV
STATISTICAL RESULTS OF MAX VOLTAGE MAGNITUDE IN CASE 1

Normal std	Max voltage magnitude		
	Maximum	mean	std
0.01	1.051	1.050	3.4×10^{-4}
0.05	1.055	1.050	1.8×10^{-3}
0.1	1.061	1.051	3.7×10^{-3}

TABLE V
STATISTICAL RESULTS OF MIN VOLTAGE MAGNITUDE IN CASE 2

Normal std	Min voltage magnitude		
	Minumum	mean	std
0.01	0.949	0.950	1.3×10^{-4}
0.05	0.948	0.950	6.7×10^{-4}
0.1	0.946	0.950	1.4×10^{-3}

C. Dynamic Performance

The 24-hour dynamic performance of the proposed TDO-VC framework is illustrated in this section. The 24-hour voltage profiles with different VVC methods are shown in Fig. 10. Serious voltage violations occur without VVC control: the maximum voltage reaches 1.15 p.u. at 13:00 during periods of high generation and low load, while the minimum voltage drops to 0.90 p.u. around 19:00 due to low generation and high demand. The situation is slightly improved in VVC control with legacy VVC devices, and the maximum observed voltage magnitude falls to 1.10 p.u. However, the legacy VVC devices alone are not able to guarantee the bus voltage within the allowed range. The bus voltages can be maintained in the allowed limits with droop control and the proposed TDO-VC, as can be seen in Fig. 10(c) and (d).

The control actions of VVC devices in the proposed TDO-VC are described in Fig. 11. When overvoltage happens, the proposed method regulates the bus voltages within the allowed range by stepping down the OLTC tap positions, and some DG inverters absorb reactive power to help reduce the voltage magnitudes simultaneously. In addition, the CB tap positions at bus 38 and 92 decrease to reduce the reactive power output to mitigate the overvoltage issue.

We further demonstrate the optimality of the proposed TDO-VC in Table VI. The table lists the average power losses over 24 hours, and the results are compared with those of the centralized method. The optimal margin of our proposed TDO-VC with centralized one is 1.3 % while this figure is 5.4 % in droop control. The performance of TDO-VC is very close to the centralized solution and much better than that in droop control, which demonstrates the effectiveness of the proposed method in minimizing power losses over 24-hour simulation.

TABLE VI
POWER LOSSES COMPARISON

Method	Losses/kW (Average)	Ratio
Centralized control	212.4	1.000
Proposed control	215.1	1.013
Droop control	223.8	1.054

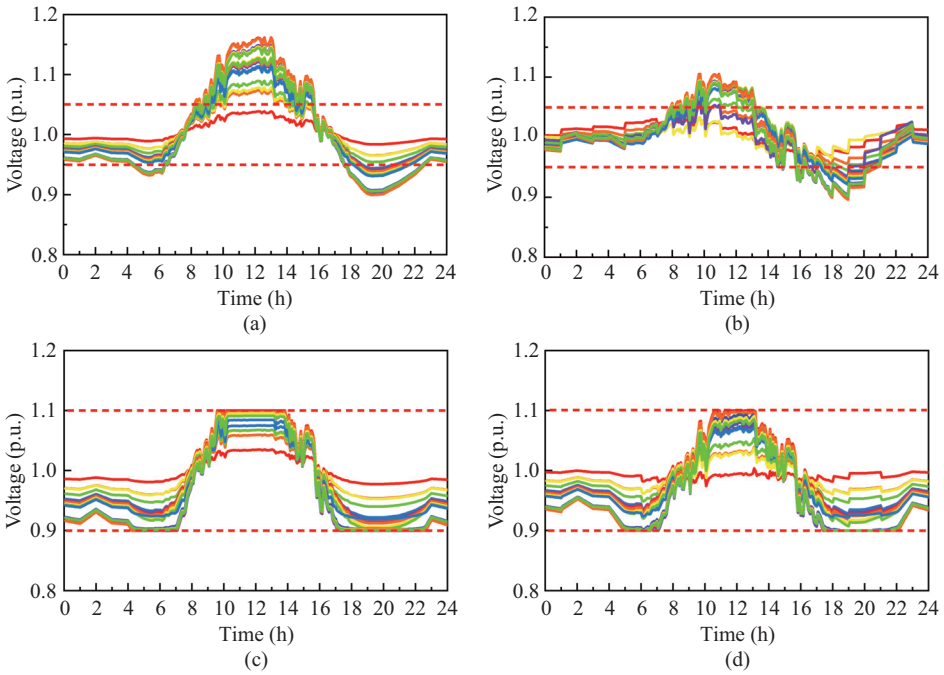

Fig. 10. Voltage profiles in different voltage control methods. (a) No voltage control. (b) Voltage control only with legacy VVC devices. (c) Droop control. (d) Proposed TDO-VC.

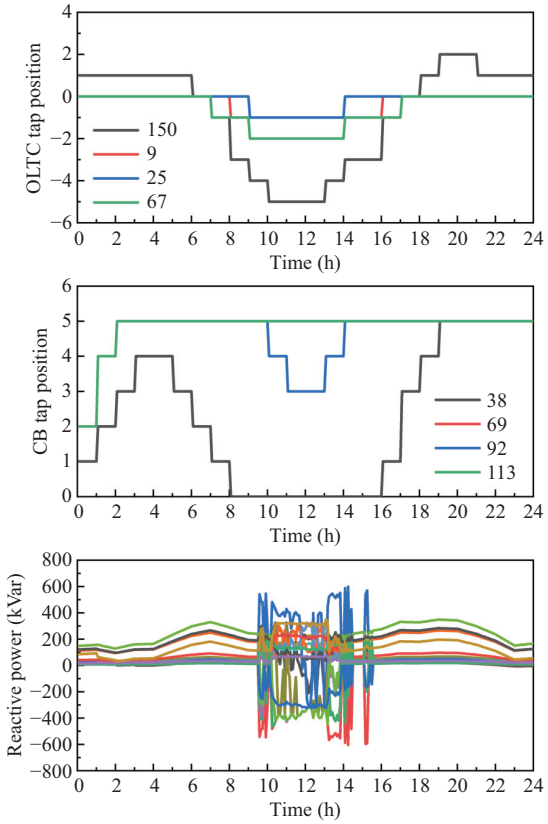

Fig. 11. Control actions.

VI. Conclusion

This paper presents a two-stage distributed online voltage control framework to address the voltage issue in distribution network with high penetration of renewable energy. The receding horizon control is applied in the upper stage to determine the control actions of mechanical voltage control devices in hourly timescale, while the reactive power outputs of DGs are dispatched in distributed and online fashion using generalized fast dual ascent. The proposed framework can be implemented online and alleviate the reliance on communication complexity. The gap to the solution in centralized solution is 1.3%, and the convergence rate is improved to $O(1/k^2)$ compared with $O(1/k)$ in dual ascent. Case studies demonstrate that the proposed TDO-VC framework outperforms other benchmark methods and it is robust to model error and communication failures. In future work, the performance of the proposed TDO-VC on unbalanced DN will be verified. In addition, the fully distributed online voltage control framework to dispatch both legacy voltage control devices and DGs will be explored.

Appendix

A. Proof of Proposition 1

Proof. Proposition 1 can be proved by the descent lemma [34, Ch.3]

B. Proof of Proposition 2

Proof. Define $\boldsymbol{\varepsilon} = [\overline{\boldsymbol{\omega}}^{\mathrm{T}}, \underline{\boldsymbol{\omega}}^{\mathrm{T}}, \overline{\boldsymbol{\eta}}^{\mathrm{T}}, \underline{\boldsymbol{\eta}}^{\mathrm{T}}]^{\mathrm{T}}$ and represent the quadratic function in the right hand of (17) as:

$$g_{\boldsymbol{L}}(\boldsymbol{\nu}, \boldsymbol{\varepsilon}) = -d(\boldsymbol{\varepsilon}) - \langle \nabla d(\boldsymbol{\varepsilon}), \boldsymbol{\nu} - \boldsymbol{\varepsilon} \rangle + \frac{1}{2}\|\boldsymbol{\nu} - \boldsymbol{\varepsilon}\|_{\boldsymbol{L}}^2 \quad \text{(B1)}$$

which implies a unique minimum

$$\boldsymbol{\nu}'(\boldsymbol{\varepsilon}) := \underset{\boldsymbol{\nu}}{\operatorname{argmin}}\, g_{\boldsymbol{L}}(\boldsymbol{\nu}, \boldsymbol{\varepsilon}) \quad \text{(B2)}$$

Assume $\boldsymbol{L} = \operatorname{blkdiag}(\boldsymbol{L}_{\overline{\mu}}, \boldsymbol{L}_{\underline{\mu}}, \boldsymbol{L}_{\overline{\lambda}}, \boldsymbol{L}_{\underline{\lambda}})$ and $\boldsymbol{L} \succeq$

$\boldsymbol{MBM}^{\mathrm{T}}$, the following inequality holds [35, Lemma 2.3]

$$-d(\boldsymbol{\nu})+d(\boldsymbol{\nu}')\geqslant\frac{1}{2}\|\boldsymbol{\nu}'-\varepsilon\|_{\boldsymbol{L}}^2+\langle\varepsilon-\boldsymbol{\nu},\boldsymbol{L}(\boldsymbol{\nu}'-\varepsilon)\rangle \quad \text{(B3)}$$

Then, we apply (B3) at point $(\boldsymbol{\nu}=\boldsymbol{\nu}^k,\varepsilon=\varepsilon^{k+1})$ and $(\boldsymbol{\nu}=\boldsymbol{\nu}^*,\varepsilon=\varepsilon^{k+1})$ respectively, and get the following two equations

$$\begin{aligned}-d(\boldsymbol{\nu}^k)+d(\boldsymbol{\nu}^{k+1})&\geqslant\frac{1}{2}\|\boldsymbol{\nu}^{k+1}-\varepsilon^{k+1}\|_{\boldsymbol{L}}^2\\&\quad+\langle\varepsilon^{k+1}-\boldsymbol{\nu}^k,\boldsymbol{L}(\boldsymbol{\nu}^{k+1}-\varepsilon^{k+1})\rangle \quad \text{(B4)}\\-d(\boldsymbol{\nu}^*)+d(\boldsymbol{\nu}^{k+1})&\geqslant\frac{1}{2}\|\boldsymbol{\nu}^{k+1}-\varepsilon^{k+1}\|_{\boldsymbol{L}}^2\\&\quad+\langle\varepsilon^{k+1}-\boldsymbol{\nu}^*,\boldsymbol{L}(\boldsymbol{\nu}^{k+1}-\varepsilon^{k+1})\rangle \quad \text{(B5)}\end{aligned}$$

Multiplying (B4) by $\gamma^{k+1}-1$ and add it to (B5) to get

$$\begin{aligned}&(\gamma^{k+1}-1)(-d(\boldsymbol{\nu}^k)+d(\boldsymbol{\nu}^*))\\&-\gamma^{k+1}(-d(\boldsymbol{\nu}^{k+1})+d(\boldsymbol{\nu}^*))\geqslant\frac{\gamma^{k+1}}{2}\|\boldsymbol{\nu}^{k+1}-\varepsilon^{k+1}\|_{\boldsymbol{L}}^2+\\&\langle\gamma^{k+1}\varepsilon^{k+1}-(\gamma^{k+1}-1)\boldsymbol{\nu}^k-\boldsymbol{\nu}^*,\boldsymbol{L}(\boldsymbol{\nu}^{k+1}-\varepsilon^{k+1})\rangle \quad \text{(B6)}\end{aligned}$$

Equation (B6) multiplied by γ^{k+1} and using the relation $(\gamma^k)^2=(\gamma^{k+1})^2-\gamma^{k+1}$ that holds in Step 3 to get

$$\begin{aligned}&2(\gamma^k)^2(-d(\boldsymbol{\nu}^k)+d(\boldsymbol{\nu}^*))-2(\gamma^{k+1})^2(-d(\boldsymbol{\nu}^{k+1})+d(\boldsymbol{\nu}^*))\\&\geqslant\|\gamma^{k+1}(\boldsymbol{\nu}^{k+1}-\varepsilon^{k+1})\|_{\boldsymbol{L}}^2+\\&2\gamma^{k+1}\langle\gamma^{k+1}\varepsilon^{k+1}-(\gamma^{k+1}-1)\boldsymbol{\nu}^k-\boldsymbol{\nu}^*,\boldsymbol{L}(\boldsymbol{\nu}^{k+1}-\varepsilon^{k+1})\rangle\\&=\|\gamma^{k+1}\boldsymbol{\nu}^{k+1}-(\gamma^{k+1}-1)\boldsymbol{\nu}^k-\boldsymbol{\nu}^*\|_{\boldsymbol{L}}^2\\&\quad-\|\gamma^{k+1}\varepsilon^{k+1}-(\gamma^{k+1}-1)\boldsymbol{\nu}^k-\boldsymbol{\nu}^*\|_{\boldsymbol{L}}^2\\&=\|\gamma^{k+1}\boldsymbol{\nu}^{k+1}-(\gamma^{k+1}-1)\boldsymbol{\nu}^k-\boldsymbol{\nu}^*\|_{\boldsymbol{L}}^2\\&\quad-\|\gamma^k\boldsymbol{\nu}^k-(\gamma^k-1)\boldsymbol{\nu}^{k-1}-\boldsymbol{\nu}^*\|_{\boldsymbol{L}}^2 \quad \text{(B7)}\end{aligned}$$

The first equality in (B7) holds by applying the Pythagoras relation $\|\boldsymbol{b}-\boldsymbol{a}\|^2+\boldsymbol{2}\langle\boldsymbol{b}-\boldsymbol{a},\boldsymbol{a}-\boldsymbol{c}\rangle=\|\boldsymbol{b}-\boldsymbol{c}\|^2-\|\boldsymbol{a}-\boldsymbol{c}\|^2$ to the right hand side with [36]

$$\boldsymbol{a}=\gamma^{k+1}\varepsilon^{k+1},\ \boldsymbol{b}=\gamma^{k+1}\boldsymbol{\nu}^{k+1},\ \boldsymbol{c}=(\gamma^{k+1}-1)\boldsymbol{\nu}^k-\boldsymbol{\nu}^* \quad \text{(B8)}$$

The second equality holds by applying the updating rule in Step 4.

By adding (B7) over iterations, we have

$$\begin{aligned}&2(\gamma^k)^2(-d(\boldsymbol{\nu}^k)+d(\boldsymbol{\nu}^*))\leqslant2(\gamma^1)^2(-d(\boldsymbol{\nu}^1)+d(\boldsymbol{\nu}^*))\\&\quad-\|\gamma^k\boldsymbol{\nu}^k-(\gamma^k-1)\boldsymbol{\nu}^{k-1}-\boldsymbol{\nu}^*\|_{\boldsymbol{L}}^2\\&\quad+\|\gamma^1\boldsymbol{\nu}^1-(\gamma^1-1)\boldsymbol{\nu}^0-\boldsymbol{\nu}^*\|_{\boldsymbol{L}}^2\\&\leqslant2(\gamma^1)^2(-d(\boldsymbol{\nu}^1)+d(\boldsymbol{\nu}^*))\\&\quad+\|\gamma^1\boldsymbol{\nu}^1-(\gamma^1-1)\boldsymbol{\nu}^0-\boldsymbol{\nu}^*\|_{\boldsymbol{L}}^2 \quad \text{(B9)}\end{aligned}$$

Given the fact that the sequence γ^k generated in Step 3 with $\gamma^1=1$ satisfied $\gamma^k\geqslant(k+1)/2,\forall k\geqslant1$. Then, we have

$$\begin{aligned}&-d(\boldsymbol{\nu}^k)+d(\boldsymbol{\nu}^*)\\&\leqslant\frac{2}{(k+1)^2}[2(-d(\boldsymbol{\nu}^1)+d(\boldsymbol{\nu}^*))+\|\boldsymbol{\nu}^1-\boldsymbol{\nu}^*\|_{\boldsymbol{L}}^2]\\&\leqslant\frac{2}{(k+1)^2}\begin{bmatrix}2\langle\boldsymbol{\nu}^*-\varepsilon^1,\boldsymbol{L}(\boldsymbol{\nu}^1-\varepsilon^1)\rangle\\+\|\boldsymbol{\nu}^1-\boldsymbol{\nu}^*\|_{\boldsymbol{L}}^2-\|\boldsymbol{\nu}^1-\varepsilon^1\|_{\boldsymbol{L}}^2\end{bmatrix}\\&=\frac{2\|\varepsilon^1-\boldsymbol{\nu}^*\|_{\boldsymbol{L}}^2}{(k+1)^2} \quad \text{(B10)}\end{aligned}$$

The second inequality holds by applying (B3) at point $(\boldsymbol{\nu}=\boldsymbol{\nu}^*,\varepsilon=\varepsilon^1)$. Further by setting $\varepsilon^1=\boldsymbol{\nu}^0$, this concludes the proof.

According to the discussions in Section IV-E, applying TDO-VC to unbalanced distribution networks inherently maintains the same convergence rate with that in this proof.

REFERENCES

[1] D. Gielen, F. Boshell, D. Saygin, M. D. Bazilian, N. Wagner, and R. Gorini, "The role of renewable energy in the global energy transformation," *Energy Strategy Reviews*, vol. 24, pp. 38–50, Apr. 2019.

[2] X. Wu, B. Zhang, M. P. Nielsen and Z. Chen, "Neural network based feasible region approximation model for optimal operation of integrated electricity and heating system," *CSEE Journal of Power and Energy Systems*, vol. 9, no. 5, pp. 1808–1819, Sep. 2023.

[3] W. Murray, M. Adonis, and A. Raji, "Voltage control in future electrical distribution networks," *Renewable and Sustainable Energy Reviews*, vol. 146, pp. 111100, Aug. 2021.

[4] Y. Xu, Z. Y. Dong, R. Zhang, and D. J. Hill, "Multi-timescale coordinated voltage/var control of high renewable-penetrated distribution systems," *IEEE Transactions on Power Systems*, vol. 32, no. 6, pp. 4398–4408, Nov. 2017.

[5] *IEEE Standard for Interconnection and Interoperability of Distributed Energy Resources with Associated Electric Power Systems Interfaces*, IEEE Standard 1547–2018, 2018.

[6] Y. Q. Dong, K. Q. Sun, J. N. Wang, S. L. Wang, H. Huang, T. Q. Liu, and Y. L. Liu, "Time-delay correction control strategy for HVDC frequency regulation services," *CSEE Journal of Power and Energy Systems*, vol. 10, no. 5, pp. 2027–2037, Sep. 2024.

[7] P. Jahangiri and D. C. Aliprantis, "Distributed volt/var control by pv inverters," *IEEE Transactions on Power Systems*, vol. 28, no. 3, pp. 3429–3439, Aug. 2013.

[8] B. S. Zhang, A. D. Domínguez-García, and D. Tse, "A local control approach to voltage regulation in distribution networks," in *Proceedings of 2013 North American Power Symposium (NAPS)*, Manhattan, KS, USA, 2013, pp. 1–6.

[9] H. J. Li, F. X. Li, Y. Xu, D. T. Rizy, and S. Adhikari, "Autonomous and adaptive voltage control using multiple distributed energy resources," *IEEE Transactions on Power Systems*, vol. 28, no. 2, pp. 718–730, May 2013.

[10] G. Cavraro, S. Bolognani, R. Carli, and S. Zampieri, "The value of communication in the voltage regulation problem," in *Proceedings of 2016 IEEE 55th Conference on Decision and Control (CDC)*, 2016, pp. 5781–5786.

[11] R. Zafar, J. Ravishankar, J. E. Fletcher, and H. R. Pota, "Multi-timescale model predictive control of battery energy storage system using conic relaxation in smart distribution grids," *IEEE Transactions on Power Systems*, vol. 33, no. 6, pp. 7152–7161, Nov. 2018.

[12] Y. F. Guo, Q. W. Wu, H. L. Gao, S. Huang, B. Zhou, and C. B. Li, "Double-time-scale coordinated voltage control in active distribution networks based on MPC," *IEEE Transactions on Sustainable Energy*, vol. 11, no. 1, pp. 294–303, Jan. 2020.

[13] Z. F. Zhang, F. F. da Silva, Y. F. Guo, C. L. Bak, and Z. Chen, "Double-layer stochastic model predictive voltage control in active distribution networks with high penetration of renewables," *Applied Energy*, vol. 302, pp. 117530, Nov. 2021.

[14] C. Zhang, Y. Xu, Z. Y. Dong, and R. Zhang, "Multi-objective adaptive robust voltage/var control for high-pv penetrated distribution networks," *IEEE Transactions on Smart Grid*, vol. 11, no. 6, pp. 5288–5300, Nov. 2020.

[15] Y. D. Huo, P. Li, H. R. Ji, H. Yu, J. L. Zhao, W. Xi, J. Z. Wu, and C. S. Wan, "Data-Driven Predictive Voltage Control for Distributed Energy Storage in Active Distribution Networks," *CSEE Journal of Power and Energy Systems*, vol. 10, no. 5, pp. 1876–1886, Sep. 2024.

[16] Q. Z. Zhang, Y. F. Guo, Z. Y. Wang, and F. K. Bu, "Distributed optimal conservation voltage reduction in integrated primary-secondary distribution systems," *IEEE Transactions on Smart Grid*, vol. 12, no. 5, pp. 3889–3900, Sep. 2021.

[17] Y. Y. Chai, L. Guo, C. S. Wang, Z. Z. Zhao, X. F. Du, and J. Pan, "Network partition and voltage coordination control for distribution networks with high penetration of distributed pv units," *IEEE Transactions on Power Systems*, vol. 33, no. 3, pp. 3396–3407, May 2018.

[18] Z. F. Zhang, F. F. da Silva, Y. F. Guo, C. L. Bak, and Z. Chen, "Distributed voltage control in distribution network with area partition," in *Proceedings of 2021 IEEE/IAS Industrial and Commercial Power System Asia (I&CPS Asia)*, 2021, pp. 646–651.
[19] G. N. Qu and N. Li, "Optimal distributed feedback voltage control under limited reactive power," *IEEE Transactions on Power Systems*, vol. 35, no. 1, pp. 315–331, Jan. 2020.
[20] J. Y. Li, C. Y. Liu, M. E. Khodayar, M. H. Wang, Z. Xu, B. Zhou, and C. B. Li, "Distributed online var control for unbalanced distribution networks with photovoltaic generation," *IEEE Transactions on Smart Grid*, vol. 11, no. 6, pp. 4760–4772, Nov. 2020.
[21] Y. F. Guo, H. L. Gao, and Z. Y. Wang, "Distributed online voltage control for wind farms using generalized fast dual ascent," *IEEE Transactions on Power Systems*, vol. 35, no. 6, pp. 4505–4517, Nov. 2020.
[22] Z. F. Zhang, F. F. da Silva, Y. F. Guo, C. L. Bak, and Z. Chen, "Coordinated voltage control in unbalanced distribution networks with two-stage distributionally robust chance-constrained receding horizon control," *Renewable Energy*, vol. 198, pp. 907–915, Oct. 2022.
[23] V. N. Lal, M. Siddhardha, and S. Singh, "Control of a large scale single-stage grid-connected pv system utilizing mppt and reactive power capability," in *Proceedings of 2013 IEEE Power & Energy Society General Meeting*, 2013, pp. 1–5.
[24] Z. Y. Tang, D. J. Hill, and T. Liu, "Fast distributed reactive power control for voltage regulation in distribution networks," *IEEE Transactions on Power Systems*, vol. 34, no. 1, pp. 802–805, 2019.
[25] Y. F. Guo, Y. X. Yuan, and Z. Y. Wang, "Distribution grid modeling using smart meter data," *IEEE Transactions on Power Systems*, vol. 37, no. 3, pp. 1995–2004, May 2022.
[26] P. Giselsson, "Improving fast dual ascent for MPC-part I: the distributed case," *arXiv preprint arXiv: 1312.3012*, 2013.
[27] B. A. Robbins and A. D. Domínguez-García, "Optimal reactive power dispatch for voltage regulation in unbalanced distribution systems," *IEEE Transactions on Power Systems*, vol. 31, no. 4, pp. 2903–2913, Jul. 2016.
[28] N. Patari, A. K. Srivastava, G. N. Qu, and N. Li, "Distributed voltage control for three-phase unbalanced distribution systems with DERs and practical constraints," *IEEE Transactions on Industry Applications*, vol. 57, no. 6, pp. 6622–6633, Nov./Dec. 2021.
[29] IEEE Distribution Test Feeder. (2017). [Online]. Available: https://cmte.ieee.org/pes-testfeeders/
[30] NREL. (2020). Solar power data for integration studies. [Online]. Available: https://www.nrel.gov/grid/solar-power-data.html
[31] Gurobi Optimization. (2020). Gurobi optimizer reference manual. [Online]. Available: http://www.gurobi.com
[32] S. Boyd, N. Parikh, E. Chu, B. Peleato, and J. Eckstein. "Distributed optimization and statistical learning via the alternating direction method of multipliers," *Foundations and Trends® in Machine Learning*, vol. 3, no. 1, pp. 1–122, Jan. 2011.
[33] H. J. Liu, W. Shi, and H. Zhu, "Distributed voltage control in distribution networks: online and robust implementations," *IEEE Transactions on Smart Grid*, vol. 9, no. 6, pp. 6106–6117, Nov. 2018.
[34] D. P. Bertsekas, *Convex Optimization Theory*, Belmont: Athena Scientific, Mar. 2009.
[35] A. Beck and M. Teboulle, "A fast iterative shrinkage-thresholding algorithm for linear inverse problems," *SIAM Journal on Imaging Sciences*, vol. 2, no. 1, pp. 183–202, 2009.
[36] C. S. Feng, B. M. Liang, Z. M. Li, W. J. Liu, and F. S. Wen, "Peer-to-peer energy trading under network constraints based on generalized fast dual ascent," *IEEE Transactions on Smart Grid*, vol. 14, no. 2, pp. 1441–1453, Mar. 2023.

Zhengfa Zhang received the B.S. and M.S. degrees in Electrical Engineering from Shandong University, Jinan, China, and the Ph.D. degree in the department of Energy from Aalborg University, Aalborg, Denmark, in 2022. From 2022 to 2023, he was a Postdoctoral Researcher with the University of Manchester, Manchester, U.K. He is currently a Postdoctoral Researcher with the University of Tennessee, Knoxville, TN, USA. His research interests include power system operation and control, with a focus on distribution network voltage control.

Filipe Faria da Silva received the M.Sc. degree in Electrical and Computer Engineering from the Instituto Superior Técnico, Lisbon, Portugal, in 2008 and the Ph.D. degree in Electric Power Systems from Aalborg University, Aalborg, Denmark, in 2011. In 2008, he was with EDP-Labelec and from 2008 to 2011, with Danish TSO Energinet. He is currently an Associate Professor with the Department of Energy Technology, Aalborg University, where he is also Semester Coordinator for the Electrical Power System and High Voltage Engineering Master Program and the Leader of the Modern Power Transmission Systems Research Program. His research interests include power cables, electromagnetic transients and insulation coordination, power quality, network stability, HVDC transmission, and HV phenomena.

Yifei Guo received the B.E. and Ph.D. degrees in Electrical Engineering from Shandong University, Jinan, China, in 2014 and 2019, respectively. He is currently a Professor with the Key Laboratory of Power System Intelligent Dispatch and Control, Ministry of Education, Shandong University, Jinan, China. From 2022 to 2024, he was a Lecturer with the School of Engineering, University of Aberdeen, Aberdeen, U.K. Earlier, he worked as a Postdoctoral Research Associate at Imperial College London, U.K., and Iowa State University, USA, from 2019 to 2022. His research interests include power system modeling, control, and optimization. Dr. Guo serves as an Assistant Editor for *International Journal of Electrical Power & Energy Systems* and an Associate Editor for *Modern Power Systems and Clean Energy.*

Yufei Xi received the B.S. and M.S. degrees in Electrical Engineering from Northeast Electric Power University, Jilin, China, in 2015 and 2018, respectively, and the Ph.D. degree in Energy Technology from Aalborg University, Aalborg, Denmark, in 2022. She was a visiting scholar at the Technical University of Munich, Germany, in 2021, and a Postdoctoral Fellow in the Department of Energy and Power Engineering at Tsinghua University from 2022 to 2024. She is currently a team leader at the Electro-Carbon Coupling Studio, State Key Laboratory of Power System Operation and Control, Tsinghua University, where she leads research on integrated energy systems, industrial green microgrids, and electro-carbon markets.

Claus Leth Bak received the B.Sc. degree (Hons.) in Electrical Power Engineering, the M.Sc. degree in Electrical Power Engineering from the Department of Energy Technology, Aalborg University, Aalborg, Denmark, in 1992 and 1994, respectively, and the Ph.D. degree in 2015 with the thesis EHV/HV underground cables in the transmission system. After his studies, he was a Professional Engineer with Electric Power Transmission and Substations with specializations within the area of Power System Protection with NV Net Transmission System Operator. In 1999, he was an Assistant Professor with the Department of Energy Technology, Aalborg University, where he is currently a Full Professor. His main research interests include corona phenomena on overhead lines, composite transmission towers, power system modelling and transient simulations, underground cable transmission, power system harmonics, power system protection, composite materials for EHV power pylons, and HVDC-VSC Offshore transmission networks. He is the Chair of the Danish Cigré National Committee, a Member of CIGRE Technical Council and Cigré SC C4 AG1. He was the recipient of the DPSP 2014 Best Paper Award, the PEDG 2016 Best Paper Award, the CIGRE Distinguished Member Award (2020), and the CIGRE TC Award (2020).

Jose Rueda Torres is currently an Associate Professor leading the research team on Dynamic Stability of Sustainable Electrical Power Systems, within the Intelligent Electrical Power Grids Section, Electrical Sustainable Energy Department, Delft University of Technology, Delft, the Netherlands. His research interests include physics-driven analysis of stability phenomena dynamic equivalence of HVDC-HVAC systems, probabilistic multi-systemic reliability and stability management, adaptive-optimal resilient multi-objective controller design.

Jin Dong received the B.S. degree from the Harbin Institute of Technology, Harbin, China, in 2010, and the Ph.D. degree from the University of Tennessee, Knoxville, TN, USA, in 2016. He is currently a Senior Research and Development Staff with the Electrification and Energy Infrastructures Division, Oak Ridge National Laboratory, Oak Ridge, TN, USA. His research interests include intersection of power systems resilience, demand response, building-to-grid integration, renewable integration, and optimal control.

Zhe Chen received the B.Eng. and M.Sc. degrees from the Northeast China Institute of Electric Power Engineering, Jilin, China, and the Ph.D. degree from the University of Durham, Durham, U.K. He is currently a Full Professor with the Department of Energy Technology, Aalborg University, Aalborg, Denmark. His research interests include wind energy and energy system integration.

Yilu Liu received the B.S. degree from Xi'an Jiaotong University, Xi'an, China, and the M.S. and Ph.D. degrees from The Ohio State University, Columbus, OH, USA, in 1986 and 1989, respectively. She is currently the Governor's Chair of The University of Tennessee at Knoxville, Knoxville, TN, USA, and the Oak Ridge National Laboratory. In 2016, she is elected as a Member of the National Academy of Engineering. She is also the Deputy Director of the DOE/NSF-cofunded by the Engineering Research Center CURENT. Prior to joining UTK/ORNL, she was a Professor with Virginia Tech, Blacksburg, VA, USA. She led the effort to create the North American Power Grid Frequency Monitoring Network, Virginia Tech, which is currently operated at UTK and ORNL as GridEye. Her research interests include power system wide-area monitoring and control, large interconnection-level dynamic simulations, electromagnetic transient analysis, and power transformer modeling and diagnosis.